Available online at www.sciencedirect.com
SCIENCE DIRECT®
ELSEVIER
Journal of Contaminant Hydrology 62–63 (2003) 287–301
JOURNAL OF Contaminant Hydrology
www.elsevier.com/locate/jconhyd

Visualization experiment to investigate capillary barrier performance in the context of a Yucca Mountain emplacement drift

Vincent C. Tidwell*, Robert J. Glass, Connie Chocas, Glenn Barker, Lee Orear

Flow Visualization and Processes Laboratory, Sandia National Laboratories, Geohydrology Department, P.O. Box 5800; Mail Stop 0735, Albuquerque, NM 87185, USA

Abstract

The use of capillary barriers as engineered backfill systems to divert water away from radioactive waste potentially stored in a Yucca Mountain emplacement drift is investigated. We designed and conducted a flow visualization experiment to investigate capillary barrier performance in this context. A two-dimensional, thin slab, test system replicated the physical emplacement drift to one-quarter scale (1.4-m diameter) and included the simulated drift wall, waste canister, pedestal, capillary barrier backfill, and host-rock fracture system. Water was supplied at the top of the simulated drift and allowed to discharge by way of wicks located along the left wall of the cell (simulated fractures) or by a gravity drain at the bottom of the right side (simulated impermeable rock with floor drain). Photographs captured the migration of water and a blue dye tracer within the system, analytical balances measured the mass balance of water, while tensiometers measured the capillary pressure at numerous locations. Of particular concern to this test was the drainage of the capillary barrier, which terminates against the drift wall. We found that while the simulated fractures (left side) and drain (right side) each influenced the performance of the capillary barrier at early time, they had little differential affect at later times. Also of concern was the small disparity in capillary properties between the fine and coarse layer (limited by the need of a fine-grained material that would not filter into the coarse layer under dry conditions). While the capillary barrier was able to divert the majority of flow toward the edges of the system and away from the simulated waste canister, the barrier did not preclude flow in the coarse layer, which was noted to be visually wet next to the waste canister on day 92 and was continuing to take on water at termination on day 112.

Keywords: Capillary barrier; Flow visualization; Capillary barrier drainage; Engineered backfill systems

* Corresponding author. Fax: +1-505-844-6023.
E-mail address: vctidwe@sandia.gov (V.C. Tidwell).

0169-7722/02/$ - see front matter © 2002 Elsevier Science B.V. All rights reserved.
doi:10.1016/S0169-7722(02)00164-X

1. Introduction

The suitability of Yucca Mountain, Nevada, as the United States' first high-level radioactive waste repository is being investigated. Licensing of this facility requires demonstration that the repository meets certain performance criteria. Demonstration of waste isolation relies both on the natural system and supplemental engineering measures. One such measure under consideration involves the use of barriers within the emplacement drifts intended to "shield" the waste canisters from water infiltrating the drift (CRWMS M&O, 1999). As part of the License Application Design Study in 1999, a capillary barrier design option was considered, and is the subject of our investigation. Although it may be reconsidered in the future, the current site recommendation design does not include the capillary barrier option.

Traditionally, capillary barriers have been used as covers for landfills and hazardous waste sites to divert water away from buried waste. Specifically, a capillary barrier consists of a layer of fine-grained porous material overlying a much coarser-grained material. Under unsaturated conditions, capillary pressures in the fine-grained layer are low relative to the entry pressure of the underlying coarse-grained layer. In this way, downward migration of water into the coarse-grained layer is impeded. If the layers are tilted, water can be diverted downdip along the interface between the two layers.

Numerous investigations have been conducted to better understand the performance aspects of capillary barriers. By way of theoretical modeling, a basis of design for capillary barrier systems has been established in which the diversion length (i.e., lateral distance water is diverted before breaching the capillary barrier) is estimated from information on the material properties, barrier slope, and recharge rate (e.g., Ross, 1990; Oldenburg and Pruess, 1993; Webb, 1997). Walter et al. (2000) used laboratory studies to test several of these models subject to a range of flow rates and barrier slopes. Conca et al. (1998) also performed laboratory experiments to investigate capillary barrier performance for uniform and offset barrier-interface conditions. Other studies have investigated the effects of heterogeneity and anisotropy (Stormont, 1995; Ho and Webb, 1998), while still others have considered how barrier geometry influences performance (Philip, 1998).

In this paper, we present the results of a two-dimensional, thin slab, laboratory experiment designed as a counterpart to fully three-dimensional pilot tests (see Webb et al., 2001) conducted to investigate capillary barrier performance in the context of a Yucca Mountain emplacement drift. According to this application, the emplacement drift, with waste canister, would be backfilled first with a coarse-grained material and capped by a finer-grained material. This capillary barrier system differs from traditional applications in two important ways. First, the diversion length is long compared to the dimensions of the drift thus raising questions concerning the drainage of water at the rock wall/capillary barrier interface. Second, the capillary disparity between the fine- and coarse-grained backfill materials is limited by the fact that the backfill may remain dry and thus rely on grain size alone to prevent the fine layer from filtering into the coarse layer. The objective of our test is to gain a better understanding of how these features influence capillary barrier performance in this unique environment.

2. Methods

2.1. Test cell and materials

The experimental system was designed to be a quarter-scale replica of a Yucca Mountain emplacement drift (Fig. 1). This entailed a test cell diameter of 1.4 m with a 40.6-cm diameter waste canister setting on a 29.3-cm tall pedestal. In cross-section, the test cell consisted of a 2.5-cm thick Lucite front faceplate (transparent), 1.25-cm thick aluminum back plate, and a 2.5-cm thick region within which the sands were emplaced. Construction of the back plate involved machining the entire test configuration from a 3.75-cm thick plate of aluminum. The Lucite faceplate was then affixed to the aluminum back plate with bolts, o-ring, and a single 'washer' plate milled to fit around the entire test cell including the waste canister and pedestal. Holes were drilled and tapped in the front Lucite faceplate as ports for the installation of tensiometers at key locations (see Figs. 1 and 2). Two ribs were added to the outside of the test cell to reduce deflection (see Fig. 2).

Selection of the capillary barrier materials used in this test was made according to their utility as future backfill for the repository. Also, selection was made such that the fine-grained material would not filter into the coarse-grained material under dry conditions. According to these needs, an Overton fine silica sand (#50–70 sieve) and a coarser crushed tuff sand (#8–20 sieve) obtained from a supplier local to Yucca Mountain were selected. The sands were introduced into the test cell with a funnel centered on the top

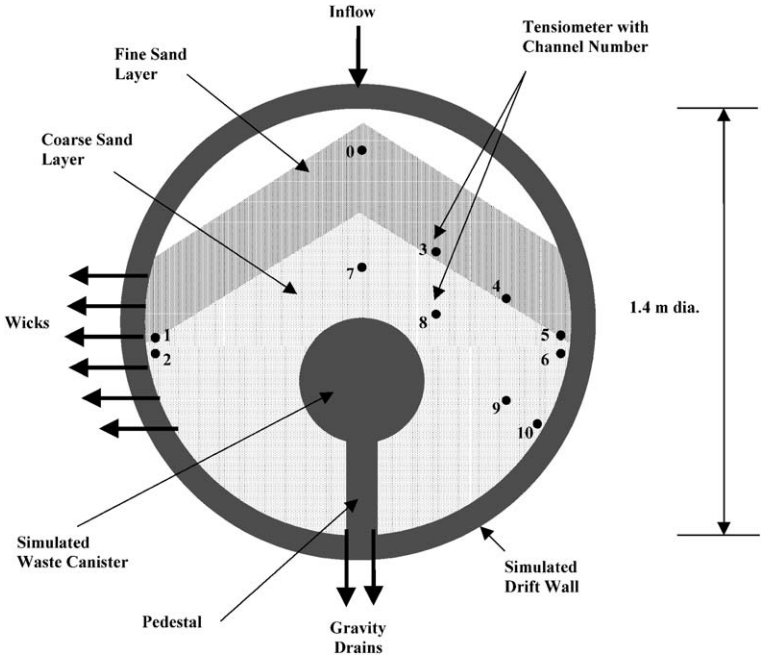

Fig. 1. Schematic of the experiment test cell showing locations of wicks (i.e., simulated fractures), drains, and tensiometers. The numbers associated with the tensiometers denote the channel.

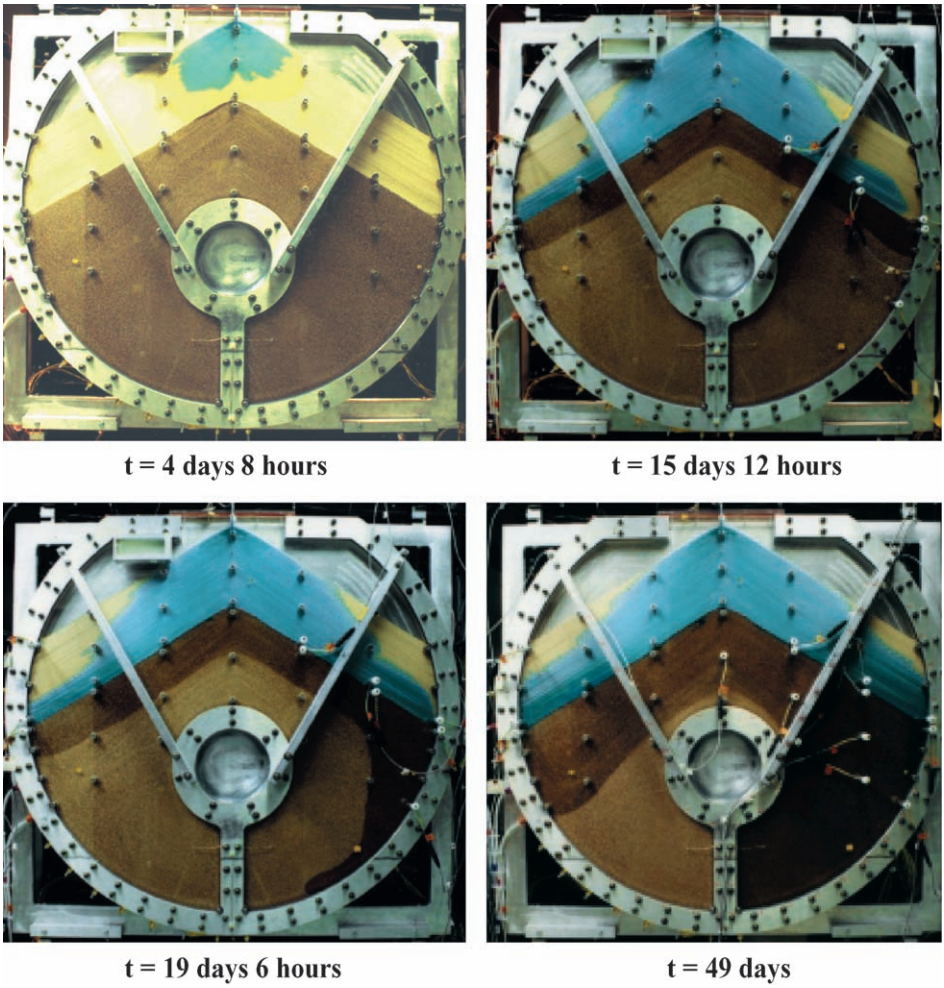

Fig. 2. Time sequence of photographs showing moisture (wet, dry) and transport pathways through the capillary barrier system. Note that blue dye was added to the test liquid to enhance visual contrast; however, some attenuation of the dye (behind the wetting front) occurred.

entry port, and were allowed to fall under the force of gravity. To mimic actual drift conditions, there was no tamping or vibration of the sand pack. The sand formed a mound directly underneath the funnel that was flanked on either side by opposite dipping slopes. The dip of the opposing slopes was approximately 30°, the natural angle of repose for these sands. The test cell was filled with coarse sand until the crown of the layer reached approximately 33 cm above the top of the simulated waste package. The Overton sand was emplaced in the same fashion to a total layer thickness of $\sim$ 28 cm. So as to not affect the underlying microstructure of the sand pack, tensiometers that protruded into the test cell were not installed until the sand pack had risen to the bottom of its port.

Table 1
Grain size distributions for backfill materials

Grain size (μm)	Coarse material (%)	Grain size (μm)	Fine material (%)
3350	0	420	6.7
2000	4.8	350	8.6
1180	59.6	300	11.0
1000	16.6	250	13.6
840	14.3	210	13.0
710	4.1	180	10.9
600	0.3	150	15.2
< 600	0.3	125	12.4
		105	4.7
		< 105	3.9

Grain size distributions for each backfill material are given in Table 1. Gross bulk densities within the cell were measured at 1.21 and 1.45 g/cm^3 for the bottom and top layers, respectively. Given the manner with which the backfill was introduced into the chamber, considerable microlayering occurred in both the fine and coarse layers (visible in Figs. 2 and 3). As such, measurement of hydraulic properties independent of the test cell would be of little use in interpreting the data. Nevertheless, calculated properties of the materials can be found in Webb et al. (2001).

The test liquid consisted of a solution of deionized water, blue dye, and potassium iodide salt. The blue dye (0.25 g/l of FD and C blue No. 1) was added to enhance visual contrast, while potassium iodide (0.8 M) was added to aid in X-ray absorption imaging (Tidwell and Glass, 1994) of the flow paths (X-ray data are not presented here). The

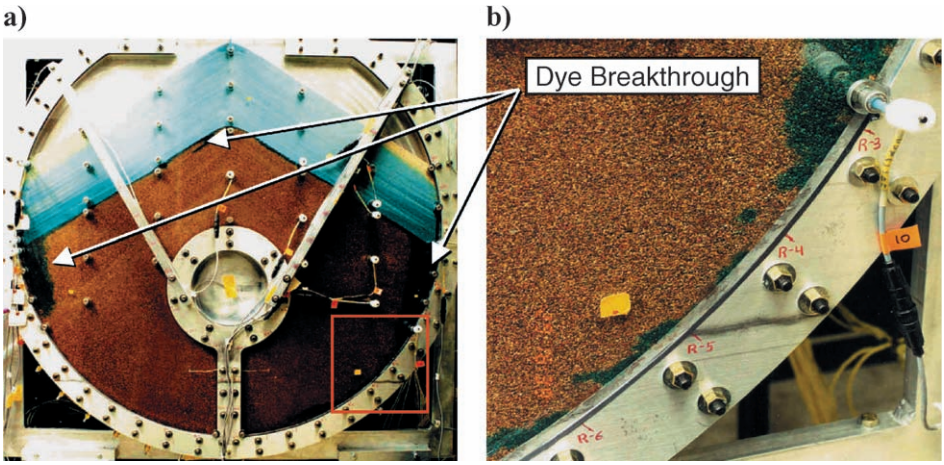

Fig. 3. Pictures showing the dye structure in the coarse-sand layer at the end of the experiment (112 days). Shown are photographs of the entire cell (a) and a close-up of the finger along the right side of the chamber (b) limited to the area designated by the red box in part (a) of this figure. Note that no fully dry regions remained within the entire cell.

density of the test liquid was 1.08 g/cm^3 while the capillary properties were found to be comparable to deionized water based on capillary rise tests.

2.2. Boundary conditions

The experiment was designed to mimic the case of a dripping fracture located at the top of an emplacement drift. Water was supplied to the initially air dry test cell using a syringe pump that discharged through a hypodermic needle located at the crown of the capillary barrier sand pack (Fig. 1). A flow rate of 0.11 ml/min, supplied in 1 ml slugs (5-s duration) every 9.5 min, was maintained throughout the 112-day test. However, two short interruptions to inflow occurred due to pump failure, one beginning 20 h after the start of the test and lasting 48 h and the second at 80 days 19 h that also lasted 48 h. The flow rate was chosen as a balance between consistency with other tests (Webb et al., 2001), time required to conduct the test, and the conditions of potential concern to the Yucca Mountain site.

Because of the symmetry of the test system, two different experiments were conducted concurrently. On the left side of the chamber, the capillary barrier was drained by way of a simulated fracture system. Along the periphery of the test cell, six wicks (0.95-cm diameter braided fiberglass, Pepperell #1380) spaced 10 cm apart were installed, three wicks in the fine sand and three in the underlying coarse sand (see Fig. 1). Each 0.61-m long wick was isolated in 1.25-cm ID clear PVC tubing with one end in contact with the sand and the other draining to an outflow reservoir. The wicks supplied suction to the chamber edge, limited by their length, as might be expected of a fracture network with similar fracture spacing. At the bottom of the left side of the test cell, a gravity drain was installed to collect any water that might pool at the bottom of the cell (i.e., not captured by the wicks). On the right side of the test cell, no wicks were installed, restricting water outflow to a single gravity drain located at the bottom of the cell.

2.3. Data acquisition

A suite of qualitative and quantitative data was collected throughout the duration of the experiment. Acquired data included the qualitative moisture and dye tracer distribution (photographs), inflow and outflow from the array of wicks and drains (balances), and the capillary pressure distribution (tensiometers). All electronic instrumentation was configured with a data acquisition system providing automatic data collection and storage. For each instrument, measurements were taken at 1-min intervals.

The transparent faceplate allowed moisture (wet or dry) and transport pathways (dye location and movement) through the capillary barrier system to be qualitatively imaged using a 35-mm camera. Photographs were taken periodically throughout the duration of the test.

Four analytic balances were used to track the mass of water in the test cell. Specifically, one analytical balance was used to measure each of the following: mass inflow, mass outflow from the fine-sand wicks, mass outflow from the coarse-sand wicks, and mass outflow from the right-side gravity drain. The outflow reservoirs and balances were housed in a sealed Lucite box to shield the balance from air currents and reduce evaporation.

Tensiometers were used to measure the water pressure at 16 different locations during the test (see Fig. 1), 11 are reported here. The tensiometers consisted of a porous cup or plate (Soil Moisture high-flow 1-bar cup and Mott 1-bar plate, respectively) held in contact with the sand pack across which the liquid pressure equilibrated, while a pressure transducer (Micro Switch Model 26PCBFA1D 0–5 psi) was used to measure the water pressure within the body of the tensiometer. The body of the tensiometer was a specially machined Swagelok fitting that could be installed through the threaded ports cut in the test cell faceplate. Porous cups that extended midway across the sand slab were used in the coarse bottom layer to establish good hydraulic connection. Flat porous plates were used in the top layer where good hydraulic connection could be made from the side of the sand layer. Calibration of the transducers was performed before and after the test.

Thermocouples were used to measure the air and liquid temperatures in and around the test cell. Measured results indicate an average temperature of 20.5 °C with a standard deviation of only 0.5 °C over the course of the experiment. The temperature was also noted to be spatially uniform. Temperature differences, on average, within the cell (top to bottom or side to side) were 0.15 °C while temperatures differed by only 0.35 °C outside the cell (top to bottom).

3. Results

The experiment was initiated on March 9, 1999 and discontinued on June 29, 1999—lasting a total of 112 days. Below, we present the results organized by wetted and dye structure development, outflow, and pressure.

3.1. Wetted and dye structure development

Fig. 2 shows a time sequence of photographs taken during the experiment. Note that the blue dye is retarded relative to the water likely due to absorption of the dye to the sand in the top layer and a combination of absorption and other processes (see Discussion) in the coarse bottom layer. Nevertheless, the position of the wetting front can generally be identified, as the color of the sand becomes darker as it wets, especially in the coarse sand.

At onset of flow, the wetted bulb grew downward until it reached the capillary barrier interface where it was deflected down along the interface. Slight asymmetry in the flow was noted during early times, which was likely caused by difficulties in delivering water precisely to the crown of the sand pack. The wetting front reached the edges of the cell at 6 (left) and 8 (right) days, respectively. After this time, wetting of the upper regions of the fine-sand layer progressed slowly.

Wetting of the coarse sand began to be noticed almost immediately after the wetting front reached the capillary barrier interface. However, progress of the wetting front in the coarse sand was much, much slower than in the fine sand initially yielding a nearly uniform wetting zone oriented normal to the capillary barrier interface. After approximately 15 days, a small bulge in the wetting front formed on the right side of the chamber against its edge (side that was not drained by wicks). With time, the bulge formed a gravity-driven finger that quickly migrated down the right wall of the test cell, reaching the

bottom of the cell at 21.25 days (average velocity of ~ 12.5 cm/day). Wetting of the coarse sand then progressed normal from the finger toward the waste canister until the entire right side was visually wetted at 37 days. On the left side of the test cell (drained by wicks simulating a fracture network), the coarse-sand layer wetted at a much slower rate. Over time, a large wavelength undulation in the wetting front formed on the left side, possibly due to gravitational instability (as on the right side) or the convergence of the flow as the front interacts with the curving wall of the test cell. The wetting front did not reach the pedestal on the left side of the chamber until 92 days.

Migration of the blue dye into the coarse sand was noted to proceed very slowly. In fact, at the end of the test (see Fig. 3), visible concentrations of dye were evident only along: the capillary barrier interface (2–3 mm into the coarse sand); one small zone close to the apex where a stringer of fine material within the coarse sand had contacted the top fine layer; two "weeps" (~ 10 cm wide) located directly beneath the capillary barrier interface along the edges of the test cell; and as a narrow finger that traversed the entire right edge of the test cell. The blue dye appeared to mark regions in the coarse sand that had conducted the majority of the flow and were possibly at higher local saturation.

3.2. Inflow and outflow data

Mass inflow and outflow data for the experiment are given in Fig. 4. The linear trend of the inflow data verifies our imposed constant injection rate. Note the two short interruptions to the fluid injection due to pump failure at 20 h and at 80 days 19 h. For

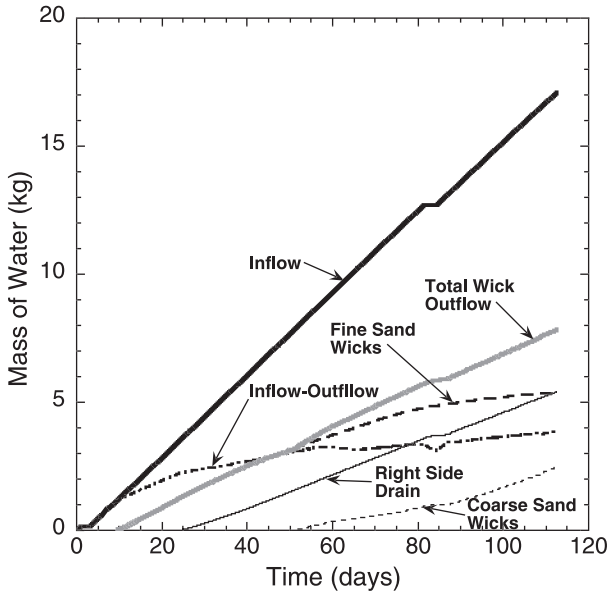

Fig. 4. Mass inflow, outflow and change in storage as measured over the duration of the capillary barrier test. For purposes of presentation, hourly data are plotted.

the left side, outflow from the fine-sand wicks began at 8 days 3 h and from the coarse-sand wicks at 51 days. For the right side, outflow from the drain at the bottom of the test cell began at 22 days 22 h. Total outflow from the left side (total wick flow) and the outflow for the single right side drain are both nearly linear; however, the curves are offset due to the additional water storage within the finger transmission zone on the right side of the chamber.

Additional dynamics of the capillary barrier system are evident in the calculated mass inflow and outflow rates (Fig. 5), in particular, differences between the two halves of the test cell. Outflow rates for the right side drain rose quickly and leveled off at approximately 80% of the half-flow rate (0.045 ml/min). However, the left side shows a more interesting dynamic due to the interaction with the simulated fracture network (i.e., wicks). The fine-sand wicks registered the first outflow, which climbed quickly to a rate slightly greater than half the inflow rate. After ~ 22 days, the outflow rate from the fine-sand wicks began decreasing and then leveled off at a rate similar to that of the right-side drain. After the coarse-sand wicks began responding at 51 days, the outflow rate from the fine-sand wicks began decreasing with a more rapid transferal of flow from fine to coarse

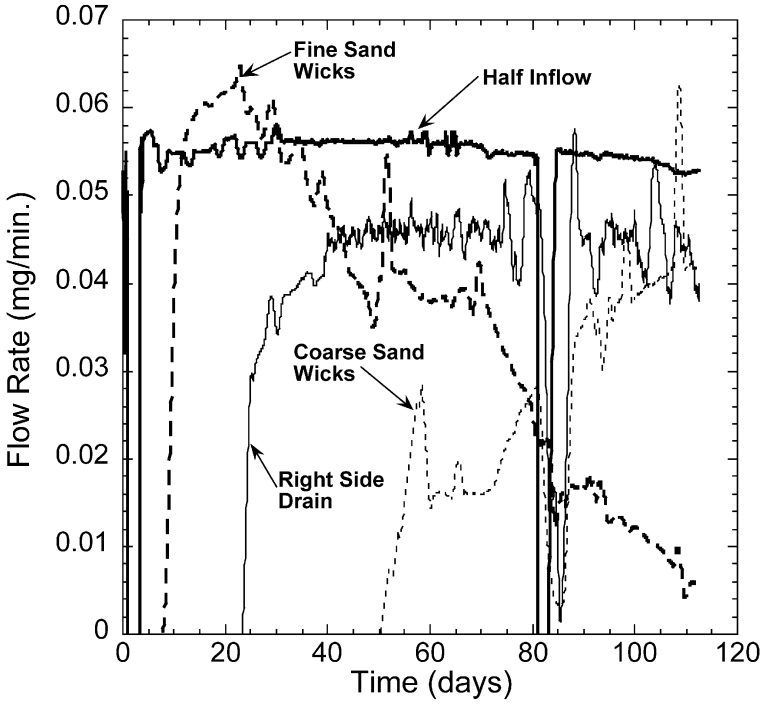

Fig. 5. Mass inflow and outflow rates measured over the duration of the capillary barrier test. Equal flow is assumed to be supplied to both sides of the cell so the half-flow rate is plotted to facilitate comparison. Data are plotted on an hourly basis with each point representing the average flow rate over a 48-h period. Spikes in the data, except those due to flow stoppage at 20 h and 81 days, are due to sagging plumbing lines that would periodically discharge (10–30 g per event).

beginning at ~ 75 days. By the end of the test, the coarse-sand wicks had captured almost all the flow from the fine sand.

From Fig. 5, we also find that the combined outflow rates for fine and coarse-sand wicks compare closely with that of the drain on the right side of the chamber (i.e., near equal outflow from the two halves of the test cell). The difference between the mass inflow and outflow for the entire cell shows that even after 112 days, the cell was wetting at a rate approximately 10% of the inflow. Calculations of potential evaporative losses from the test system are much smaller than the difference between inflow and outflow thus confirming this continued long-term wetting.

3.3. Tensiometer response

Fig. 6 shows the response of tensiometers located in the fine-sand layer (see Fig. 1). Near the injection point (Channel 0), water pressure remained quite stable at ~ −50 cm throughout the experiment. The earlier arrival of the wetting front at the left edge (Channel 1) versus the right edge (Channel 5) is clearly seen. Interestingly, the behavior of locations

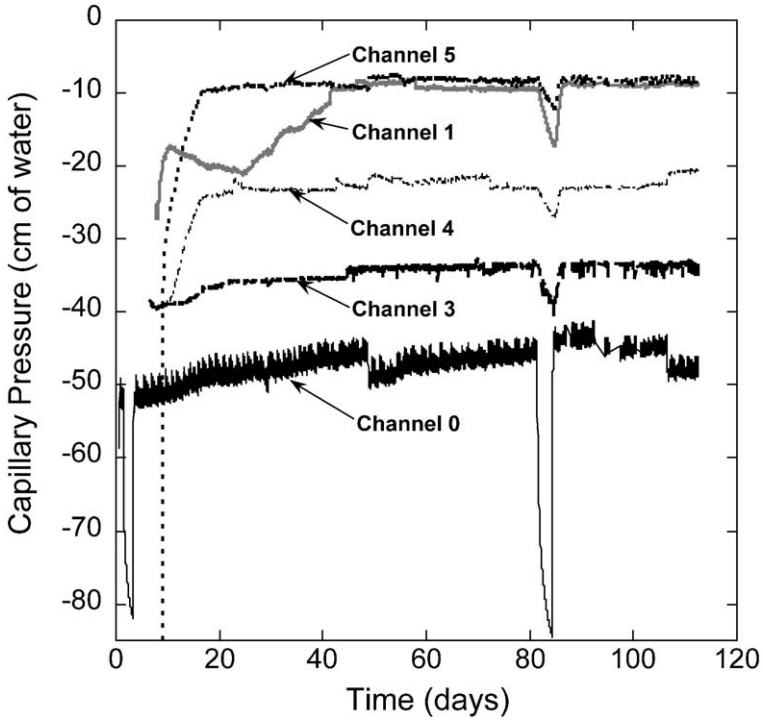

Fig. 6. Water pressure data measured with tensiometers located in the fine-sand layer. Note that tensiometers were not primed until the wetting front approached the sensor. The sharp pulses noted in several of the tensiometer readings mark times when the tensiometers were re-primed. For purposes of presentation, hourly data are plotted. The apparent diurnal pattern exhibited by Channel 0 is an aliasing artifact resulting from the plotting of hourly data.

on either side of the chamber is very different after arrival. While the right rises rapidly to approximately −10 cm and remains roughly constant for the remainder of the test, the left side, where wicks are present (i.e., simulated fracture network), pressure slowly decreases after arrival (days 10 to 25) followed by a slow increase to near identical pressures as on the right side (day 45). For the left side, the decrease in pressure is associated with the enhanced outflow (higher than half inflow) from the fine-sand wicks during the same time period. When pressure begins to decrease, outflow begins to decrease and reaches the same outflow as the right side at 45 days when the pressures are identical. Also evident is the distinct increase in pressures from the inlet (Channel 0) to channels 3, 4, and 5 indicating an increase in saturation as one traverses the flow path along the capillary barrier interface.

Water pressures for locations in the coarse-sand layer are plotted in Fig. 7. The time series for each channel show a rapid increase in pressure with the approach of the wetting front that smoothly transitions to a relatively constant value after the front passes. This transition is sharp for tensiometers near the edge of the test cell while becoming broader or more diffuse as one moves away from the edge towards the inside of the cell. We also see that the highest pressures (highest liquid saturations) are found along the outside edge of

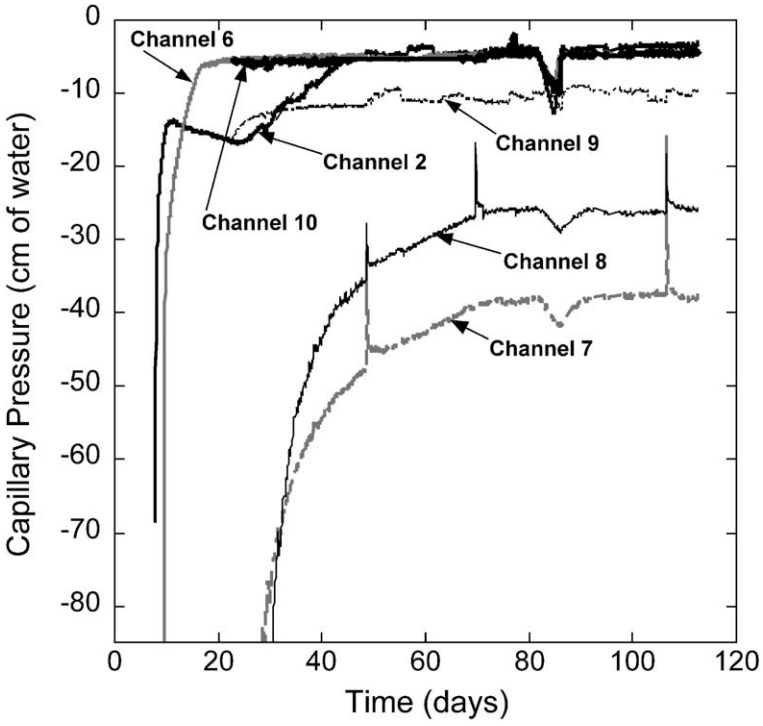

Fig. 7. Water pressure data measured with tensiometers located in the coarse-sand layer. Note that tensiometers were not primed until the wetting front approached the sensor. The sharp pulses noted in several of the tensiometer readings mark times when the tensiometers were re-primed. For purposes of presentation, hourly data are plotted.

the test cell (Channel 10). Moving away from the simulated drift wall, the pressures sequentially decrease from ~ -5 cm (Channel 10) to ~ -10 cm (Channels 9), ~ -24 cm (Channels 8) and finally ~ -38 cm (Channel 7).

Finally, we note that the two periods of time when injection stopped are clearly seen as decreased pressure directly below the injection point (Channel 0) followed by rebound back to the earlier value once flow was reinstated. For the second period at 82 days, we see rapid pressure response on interruption at all measured locations. In contrast, on reinstating flow, recovery times appear to increase with distance from the inlet. On a consistent basis, the pressure data for Channel 0 exhibit a distinct periodicity, correlated with the fluid injection schedule; however, this effect is damped out before it reaches any of the other ports.

4. Discussion

The capillary barrier system of interest to the emplacement drift environment differs from traditional applications in two important ways. First, the diversion length is long compared to the dimensions of the drift and thus interaction with the walls and its fracture network is of primary concern. Second, the capillary disparity between the fine and coarse grained backfill materials is limited by the fact that the backfill may remain dry and thus rely on grain size alone to prevent the fine layer from filtering into the coarse layer. In light of the acquired data, the behavior of the capillary barrier system with regards to these two features can now be discussed.

Like the capillary barrier in our experiment, those for use at Yucca Mountain would be designed such that the diversion length for the system is greater than the radius of the drift. In this regard, our experiment elucidates the expected behavior of a system foreshortened by the interaction of the diverted water with the edge of the drift. In the experiment, two possibilities were investigated, one with a simulated fracture network, the other with an impermeable drift wall and bottom floor drain. This difference is seen to have considerable effect on the early time wetting history of the capillary barrier. Flow on the left side, with the simulated fracture network, is almost entirely captured by the wicks. In contrast, flow on the right side was conveyed to the bottom of the cell and out the gravity drain by way of a gravity-driven finger formed along the cell edge.

The difference in barrier performance in the presence and absence of the simulated fracture network is further emphasized in Figs. 6 and 7. There we find the tensiometers associated with Channels 5 and 6 on the right side to show a monotonically increasing pressure with time while Channels 1 and 2 (near the wicks) do not. These two different responses verified that the two sides of our experiment acted independently, as designed, with minimal hydraulic connection. The decrease in pressure at the wicks after the initial increase coincides with enhanced outflow from the fine sand (above half the inflow rate, Fig. 5) and is likely due to the action of the wick as a ‘capillary siphon’ similar to that created by gravity-driven fingers within individual fractures or porous media (Glass and Nicholl, 1996). However, for some reason, this capillary siphon is ‘broken’ at 25 days causing a slow increase in the pressure up to values identical to the right side (at 50 days). This increase is also associated with the slow failure of the capillary barrier on the left with

flow from the coarse-sand wicks ultimately taking nearly the entire left side outflow by the end of the test.

In contrast, by the end of the test, little difference in the two sides of the test cell was distinguishable. That is, both sides of the test cell were wetted and the capillary pressure conditions at the barrier interface/cell wall were nearly identical (Channels 1–2 and 5–6). It is apparent that some means of draining the water from the system is necessary. What is uncertain is how important the relative strength and position of the drains (i.e., unsaturated fractures) are in the long-term performance of the system.

The small disparity in capillary properties between the fine and coarse layers arises from the need to have a stable sand pack under dry conditions (i.e., fine layer materials will not filter into coarse layer). On the positive side, the photographic, outflow, and water pressure data suggest that flow on both sides of the chamber moves primarily along the capillary barrier interface in the fine-sand layer to the edges of the chamber. That is, the capillary barrier effectively diverted the majority of flow away from the waste package region. Less favorable was the fact the capillary barrier did not isolate the waste canisters from water. In fact, the entire chamber had wetted to some degree by day 92 bringing water, albeit a very small volume, in contact with the waste canister. Wetting occurred primarily out from the gravity driven finger on the right side of the chamber and uniformly down from the capillary barrier interface on the left side drained by the wicks. Even at 112 days, the capillary barrier system was continuing to wet at a rate $\sim$ 10% of the inflow rate (bulk saturation of the entire test cell at the end of the test was estimated at $\sim$ 25%). This stands in contrast to the results of Conca et al. (1998) in which no distinguishable wetting of the coarse layer occurred in a year's time, albeit for a barrier system with considerably greater disparity in capillary properties.

The wetting of the coarse layer raises a number of questions about system performance. First, what are the mechanisms responsible for water transport in the coarse layer? The lack of blue dye within the majority of the coarse layer where we believe the increase in saturation to be occurring is suggestive of two possible flow processes: film flow along the edges of grains and/or vapor transport, i.e., the large organic molecule would be filtered by thin films or left behind when water evaporates. Second, how mobile is the water in the coarse layer? If the test had been conducted longer, it is possible that the pathways conducting the majority of the flow (wicks on the left and gravity finger on the right) may have changed or widened as overall saturation increased. However, it is equally likely that, at least along the right side, the gravity-finger would have persisted indefinitely due to hysteretic mechanisms (Glass et al., 1989). Of additional interest is the small width of the conducting zone of the gravity finger (see Fig. 3b), substantially narrower than the zone originally darkened by the growing finger (see Fig. 2, 19 days 6 h). Near the waste canisters, one might expect flow to be essentially stagnant; at least once the system reaches equilibrium. Even if this were the case, the presence of water could enhance waste package corrosion and/or potentially enhance diffusion of radionuclides through the backfill.

In context of the larger, full drift scale system, we interpret our results directly though the use of the capillary similitude scaling theory of Miller and Miller (1956). Assuming that the flow processes occurring within our test are governed by standard unsaturated flow physics as embodied in Richard's equation, then similitude theory requires that the distributions in log space of grain size about the mean for each layer remains the same. In

essence, this requirement simply restricts the pore scale geometry within the capillary barrier system to be geometrically similar. Now the mean grain sizes for the drift scale backfill, $\langle d_d \rangle$, can be scaled to those in the experiment, $\langle d_{exp} \rangle$, by the relation:

$$\frac{L_{exp}}{L_d} = \frac{\langle d_d \rangle}{\langle d_{exp} \rangle}$$

where L_{exp} and L_d are the macroscopic scales (say the diameter) of the experiment and drift, respectively. In addition, the time can also be scaled with

$$\frac{t_{exp}}{t_d} = \frac{\langle d_d \rangle}{\langle d_{exp} \rangle} \left(\frac{L_{exp}}{L_d} \right)^2$$

Making use of these simple scaling relations and others for the pressure and applied fluxes allows the results of our test to directly simulate those of the full drift scale system.

Finally, we would like to note that the properties within our capillary barrier system were far from uniform. Stringers of fine-grained materials (silt and very fine-grained sand) were evident throughout both the fine- and coarse-sand layers in our experiment. These laminae, formed by fractionation as the sand was poured into the cell, are largely oriented parallel with the capillary barrier interface and concentrated near the outer edge. Such microlayering has been considered to yield an effective moisture-dependent anisotropy in naturally occurring dune deposits (McCord et al., 1991). Photographs of the wetting process suggested that these heterogeneities influenced the wetting primarily within the fine-sand layer, where the wetting front appears to move faster in some laminae relative to others.

5. Concluding remarks

This experiment provides important insights into the performance of a capillary barrier system within the context of a waste repository drift. However, additional research is necessary to determine whether capillary barriers represent a viable engineered backfill solution. In particular, the relatively rapid wetting of the coarse-sand layer suggests that the selected test materials are far from optimal. Also, this test was run with a tersely conceptualized drainage system. As barrier drainage will play an important role in system performance and design, the natural fracture system needs to be characterized and then tested with respect to potential design scenarios. Additional consideration and separation of processes that wet the bottom layer such as vapor phase transport and film flow also must be accomplished, as these poorly understood processes could have a profound influence, potentially over large time scales. We also note that the emplacement of any backfill material in a repository drift is sure to introduce textural and material property heterogeneities into the capillary barrier system, the effects of which must be considered. Finally, tests should be run to consider thermal effects on long-term capillary barrier stability. In this case, adding the thermal load of a waste package may compensate for the

slow wetting of a surrounding coarse layer and thus improve the performance of the barrier.

Acknowledgements

We acknowledge Craig Boney, Nick Teske and Jerry Jones for helping in putting the experiment together, reducing data, and assembling data plots. This work was supported by the US Department of Energy's, Office of Civilian Radioactive Waste Management (design and conduct of experiment) and Office of Basic Energy Science, Geoscience Research Program (manuscript preparation), under contract DE-AC04-94AL85000. Sandia is a multiprogram laboratory operated by Sandia Corporation, a Lockheed Martin Company, for the United States Department of Energy. Data referenced in this paper are available from the YMP Site and Engineering Properties Data Base under Data Tracking Numbers SN0004L1011398.004, TDIF#310419 and SN0004L1011398.005, TDIF#310420.

References

Conca, J.L., Apted, M.J., Zhou, W., Arthur, R.C., Kessler, J.H., 1998. Flow barrier system for long-term high-level waste isolation: experimental results. Nucl. Technol. 124 (1), 1–13.

CRWMS M&O, 1999. Engineered Barrier System Performance Testing for Site Recommendation and License Application: Activity Evaluation. June 23, 1999. CRWMS M&O, Las Vegas, NV.

Glass, R.J., Nicholl, M.J., 1996. Physics of gravity driven fingering of immiscible fluids within porous media: an overview of current understanding and selected complicating factors. Geoderma 70, 133–163.

Glass, R.J., Steenhuis, T.S., Parlange, J.-Y., 1989. Mechanism for finger persistence in homogeneous unsaturated porous media: theory and verification. Soil Sci. 148, 60–70.

Ho, C.K., Webb, S.W., 1998. Capillary barrier performance in heterogeneous porous media. Water Resour. Res. 34 (4), 603–609.

McCord, J.T., Stephens, D.B., Wilson, J.L., 1991. Hysteresis and state-dependent anisotropy in modeling unsaturated hillslope hydrologic processes. Water Resour. Res. 27 (7), 1501–1518.

Miller, E.E., Miller, R.D., 1956. Physical theory for capillary flow phenomena. J. Appl. Phys. 27, 324–332.

Oldenburg, C.M., Pruess, K., 1993. On numerical modeling of capillary barriers. Water Resour. Res. 29 (4), 1045–1056.

Philip, J.R., 1998. Seepage shedding by parabolic capillary barriers and cavities. Water Resour. Res. 34 (11), 2827–2835.

Ross, B., 1990. The diversion capacity of capillary barriers. Water Resour. Res. 27 (10), 2625–2629.

Stormont, J.C., 1995. The effect of constant anisotropy on capillary barrier performance. Water Resour. Res. 31 (3), 783–785.

Tidwell, V.C., Glass, R.J., 1994. X-ray and visible light transmission for laboratory measurement of two-dimensional saturation fields in thin-slab systems. Water Resour. Res. 30 (11), 2873–2882.

Walter, M.T., Kim, J.-S., Steenhuis, T.S., Parlange, J.-Y., Heilig, A., Braddock, R.D., Selker, J.S., Boll, J., 2000. Funneled flow mechanisms in a sloping layered soil: laboratory investigation. Water Resour. Res. 36 (4), 841–849.

Webb, S.W., 1997. Generalization of Ross' tilted capillary barrier diversion formula for different two-phase characteristic curves. Water Resour. Res. 33 (8), 1855–1859.

Webb, S.W., George, J.T., Finley, R.E., 2001. Pilot-scale evaluation of engineered barrier systems for the Yucca Mountain project. Proceedings of the 38th U.S. Rock Mechanics Symposium, Washington, D.C., July 7–10. Balkema, Rotterdam, pp. 605–612.